N92-21907

Crab Pulsar Giant Pulses: Simultaneous Radio and GRO Observations

Scott C. Lundgren and James M. Cordes (Cornell University)
Roger Foster (NRL)
Tim Hankins (NMMT and NRAO,VLA)
Mel Ulmer (Northwestern University)
Chris Garasi (Case Western Reserve University)

Abstract

We report observations of the Crab pulsar made at radio frequencies concurrent with OSSE observations from 15 to 27 May 1991. Using the 43 m telescope at Green Bank at 0.8 and 1.4 GHz, we sampled continuously for 10 hours per day at intervals of 100 to 300 microseconds. Our analysis of the radio data includes calculation of histograms of pulse intensities, absolute timing to about 20 microsecond precision, and characterization of intensity variations on time scales from the 33 ms spin period to days. We present the most detailed analysis made of giant pulses. The ultimate goal is to bin the radio data into giant and non-giant pulses and to form average waveforms of OSSE data for the corresponding pulse periods. We will thereby test whether the violent radio fluctuations (which are not seen in other radio pulsars to the same degree) are correlated with low energy gamma-rays, yielding constraints on the radio coherence mechanism and the steadiness of the electron-positron outflow in the magnetosphere. Timing analysis of our radio data provides a well defined ephemeris over the specified range of epochs, including a contemporaneous measurement of the dispersion measure. We can predict the gamma-ray pulse phase with an error of less than $70\mu s$.

Introduction

Giant radio pulses from the Crab pulsar have been observed almost since its discovery (Heiles, Campbell, Rankin 1970; Staelin and Sutten 1970). Both the main and interpulses exhibit this phenomenon, but not the precursor component (Gower and Argyle 1972; Argyle 1973). The long tail on the pulse energy histogram distinguishes the Crab fluctuations from all other pulsars. The modulation index (ratio of average fluctuations to average level) of unity measured for the Crab is comparable to many other pulsars (Bartel, Sieber, Wolszczan 1980). However, the Crab modulations span many orders of magnitude, while pulse energy histograms for other pulsars show a maximum energy of 10 times the average. Typical pulsars have Gaussian or exponential pulse energy histograms (Hesse and Wielebinski 1974). For observable individual pulses, the Crab pulse energy histogram obeys a power law.

A variety of mechanisms cause pulse energy modulations on time scales of a few to many pulse periods. Diffractive scintillations due to turbulence in the interstellar plasma cause fluctuations with a decorrelation bandwidth on the order of 100 kHz for the Crab at 800 MHz (Manchester and Taylor 1977). In our observations with a 20 MHz bandwidth, these modulations are quenched. Other mechanisms seem to be intrinsic modulations in the effectiveness of the emission mechanism. Many pulsars display pulse nulling in which the emission turns off entirely for many consecutive pulse periods (Ritchings 1976). Switching a coherence mechanism on and off may cause these nulls. Alternatively, an enhancement or suppression of pair creation may influence the radio emission. Other pulsars switch between two different emission modes (Backer 1970). In such cases, the average profile switches between two shapes depending on observation time. Since most Crab pulses are hidden by the brightness of the nebula background, it is not clear whether giant pulses are caused by a different mechanism from smaller pulses, or they are simply an extension of a continuous distribution of pulse energies.

Simultaneous observations of the Crab pulsar at gamma-ray and radio wavelengths will distinguish between enhanced pair cascade and radio coherence mechanisms for giant pulse emission. Changes in pair production efficiency would affect both radio and gamma-ray emission. On the other hand, improved radio coherence would have no effect on gamma-ray emission. The long term goal of this project is to compare gamma-ray emission of the Crab during giant pulses and lesser pulses, in the hope of constraining emission mechanism theories for young pulsars.

Observations

For our radio observations of the Crab pulsar, we used the spectral processor at the NRAO's Green Bank 43 m telescope at 1330 MHz for 2 days, at 800 MHz for 1 day and at 812.5 MHz for 10 days. We sampled every 200 μs or 300 μs in hour long scans 10 hours per day (May 15-27). This resulted in 24 Gbytes of data containing over 10^7 pulse periods and 3×10^4 giant pulses.

At radio frequencies, interstellar plasma dispersion delays lower frequency signals with respect to higher frequencies, thus smearing a pulsed signal. To remove this effect, the spectral processor divides the 20 MHz bandwidth into 256 channels and compensates for the relative delays between channels to dedisperse the signal using the known dispersion measure of the Crab pulsar. This reduces the dispersion smearing from 18 ms across 20 MHz at 800 MHz to 70 μs across each 78 kHz channel. The spectral processor provides intensity outputs in individual polarizations and in two contiguous bandpasses of 10 MHz each. Pulsar pulses could be discriminated from interference by requiring that the correct dispersion delay appear in spikes that occur in the two 10 MHz bandpasses.

Data Analysis and Results

We developed analysis software to produce average pulse profiles and to extract giant pulses from the fast sampled data. Due to Earth rotation, orbital motion, and pulsar spindown, the pulsar period changes significantly over an hour long observation. The program TEMPO (from J.H. Taylor) calculates the topocentric period behavior given input parameters for the pulsar period, period derivative, and sky position. Our program uses pulse phase prediction from TEMPO in creating average profiles.

To quantify giant pulse behavior, we calculated an average fluctuation profile in addition to the average profile (fig. 1a). With no variation in pulse intensity the fluctuation average would be zero. The modulation index (ratio of fluctuations to the average) is determined by the intensity distribution of giant pulses. Typically for the Crab pulsar, the ratio of the fluctuation waveform to the mean waveform is near 1, indicating that the intensity is 100% modulated. Most of this modulation comes from giant pulses. In fact, in several of our hour averages, a single giant pulse more than 400 times the average increases the modulation index to more than 8. By contrast, optical measurements (Hegyi, Novick and Thaddeus 1971) place an upper bound of 1% on pulse to pulse fluctuations.

While most individual pulses are not observable (signal to noise ratio S/N=0.07), individual giant pulses may greatly exceed the noise (fig. 1b). This allows us to extract the area ('pulse energy'), arrival time and width for each giant pulse above the noise in our data. By designating giant pulses as only spikes with the correct dispersion offset between the lower 10 MHz band and the upper 10 MHz band, we lowered the giant pulse flux threshold to 3 sigma or 0.1 times the nebula without introducing spurious giant pulses.

By cross correlating each average profile with a high signal to noise template we calculated precise arrival times from each average profile. The program TEMPO references these topocentric arrival times to the Solar System barycenter. By fitting barycentric arrival times to a model, the program provides current values for the pulsar period and spindown. From the offset between 1330 MHz
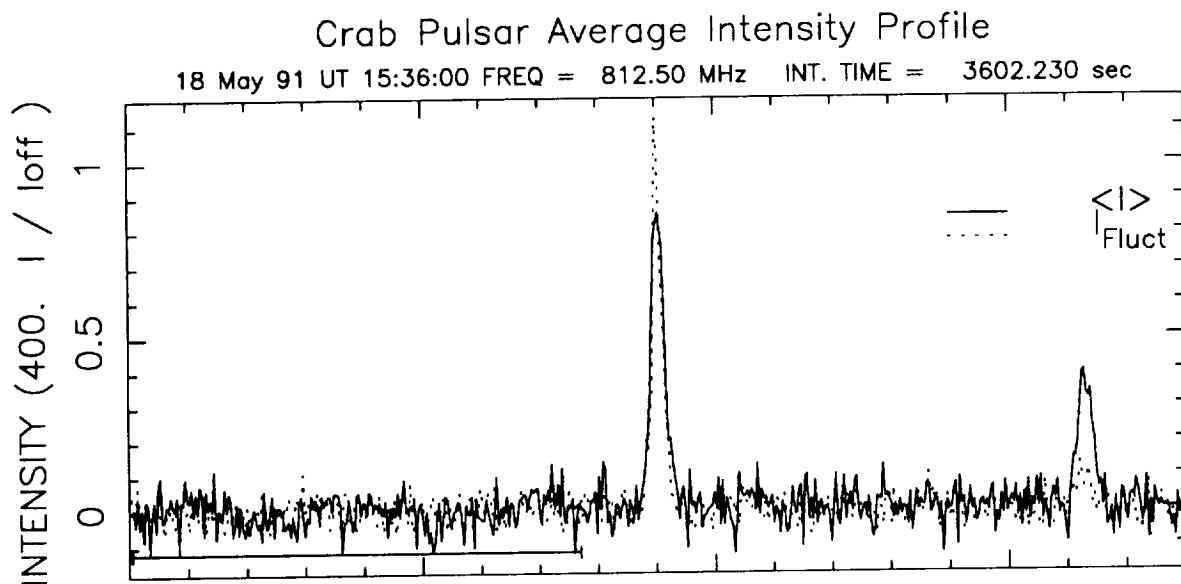
Crab Pulsar Average Intensity Profile
18 May 91 UT 15:36:00 FREQ = 812.50 MHz INT. TIME = 3602.230 sec

Figure 1a shows a typical average profile from one hour of data. The solid line average profile is centered on the main pulse. On this intensity scale 400 corresponds to the intensity of the Crab Nebula, the background from which dominates the system temperature. The dotted line fluctuation average $((< I^2 > - < I >^2)^{0.5} - \sigma_{OffPulse})$ indicates the presence of giant pulses.

Giant Pulse Average
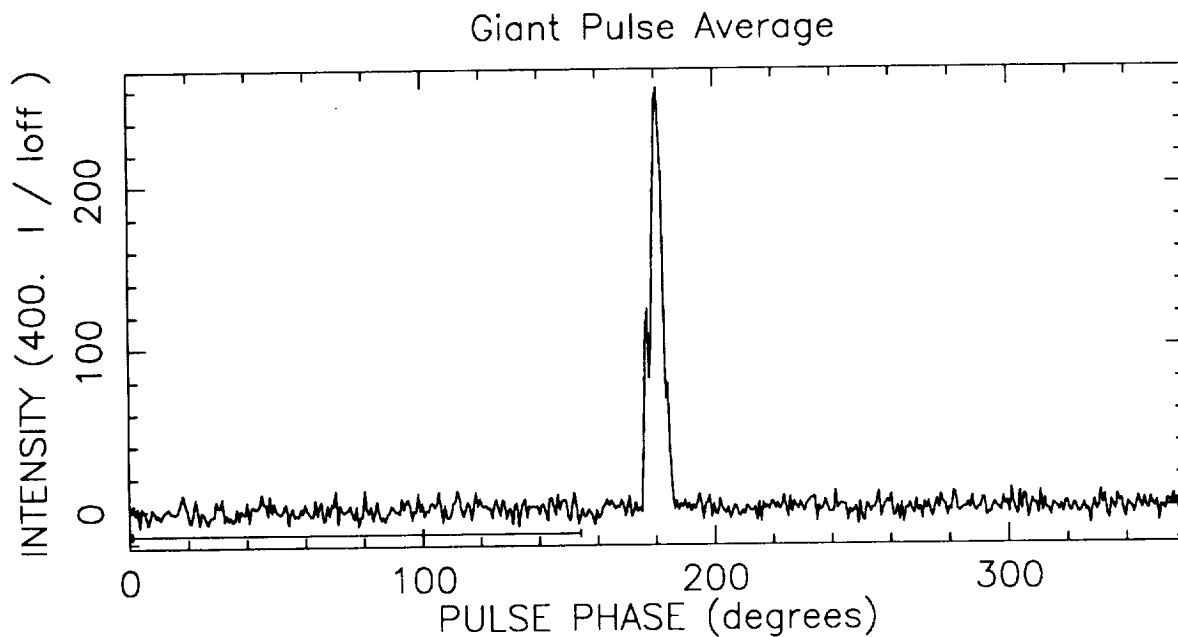
Figure 1b shows a sub-average which includes only giant main pulses above a threshold of 200 in our units. An average of 15 of these occur per hour.

and 812.5 MHz arrival times, we fit for dispersion measure (DM) as well. An accurate dispersion measure is necessary to compare radio pulse arrival times (delayed by the interstellar plasma) to gamma-ray arrival times (unaffected by dispersion).

We used the 10 days of 812.5 MHz data to fit for period and period derivative, holding period second derivative fixed to the known value. Then, while holding these fixed, we added the 1330 MHz data to fit for DM. This resulted in the following parameters:

$$
\begin{array}{lll}
P = 33.3264436338 \text{ ms} & \text{or} & \nu = 29.9483705571866 \\
\dot{p} = 419.4132 \times 10^{-15} ss^{-1} & & \dot{\nu} = -3.77628 \times 10^{-10} \\
\text{pepoch} = 46625.5 \text{ (jd)} & & \text{epoch} = 48403 \\
& \text{DM} = 56.776 \pm 0.005 &
\end{array}
$$

Our DM accuracy allows conversion to infinite frequency arrival times to within 70 μs.

The rms residual for the average profiles is 20 μs (fig. 2a). Giant pulses, on the other hand, are spread over $\pm 300 \mu$s. Since this spread is much larger than the 205 μs or 307.5 μs sample interval used, we attribute it to intrinsic jitter in arrival times. The offset between the average giant pulse residual and the average profile residual agrees with zero within the errors (6 μs $\pm$ 3 μs).

The number of giant pulses varies from day to day. During the first two days, we observed at 1330MHz. The pulsar signal is much weaker at this frequency, so we saw many fewer giant pulses above the noise threshold. However, even at a single frequency, the rate of giant pulses varies. For example, giant pulses were much less frequent on day 48400 than they were on day 48402.

To describe the time distribution of giant pulses (fig. 3), we postulated that the mechanism is a Poisson process. This requires that each giant pulse is statistically independent of every other giant pulse. Rotation of the pulsar beam through our line of sight samples the Poisson process at discrete intervals determined by the period. Sampling an exponential distribution of times at integer multiples of the period gives a histogram which agrees well with our observations. The small deviations observed will require more detailed future analysis to determine their significance. Overall, the giant pulses are randomly distributed in time.

We also examined the energy distribution of giant pulses at 812.5 MHz. The giant main pulse energy histogram in figure 4 displays a steep power law distribution (index=-3.46 $\pm$ 0.04). This is significantly steeper than the -2.5 power law found by Argyle at 146 MHz (Argyle and Gower 1974), suggesting that the giant pulse mechanism is less efficient at higher frequencies. The largest giant pulse measured in 2 weeks was 12.5 times the nebula flux or 5000 times the average main pulse flux! The roll off at low energies is most likely due to our noise thresholding. Hankins has made high time resolution observations at the Very Large Array (VLA). These observations resolve giant pulse fine structure into multiple 10 μs spikes. Earlier work determined an exponential decay time scale for spike energy of 90 μs at 430 MHz (Hankins and Rickett 1975) that is caused by interstellar scattering.

Future Work

For each giant pulse in our data we have the arrival time, the width and energies for that pulse, the interpulse, the next pulse and interpulse, and the previous pulse and interpulse. From correlations between arrival times, rates, widths and energies we hope to constrain theoretical models for giant pulse emission mechanisms. Additionally, we will cross-correlate our data with gamma-ray data from GRO. We will provide our giant pulse barycentric arrival times to the GRO community. These times can be converted to spacecraft arrival times. Averages of those gamma-ray pulses which correspond to giant radio pulses can then be formed and compared to non-giant
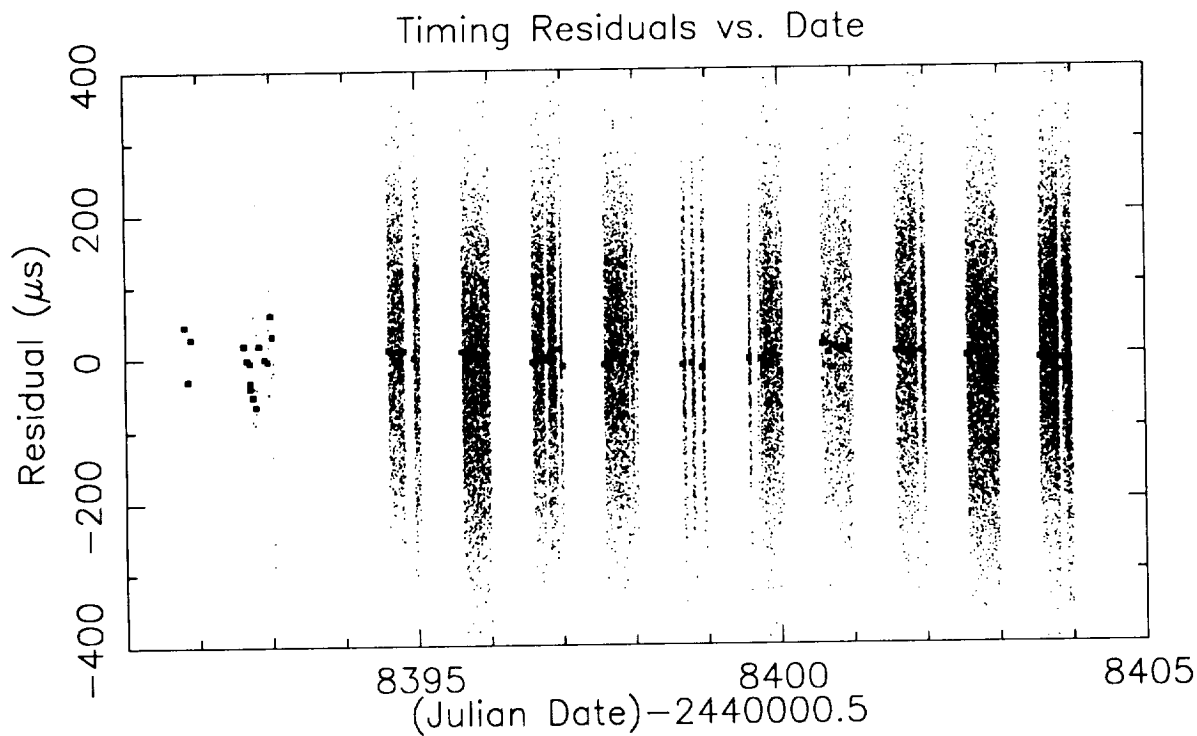
Timing Residuals vs. Date

Figure 2a We have plotted the residuals from our timing fit. The large squares correspond to residuals for the average profiles. On the same plot we included residuals for the individual giant pulse arrival times, as small dots. Blank strips in the plot correspond to times when we were not observing.
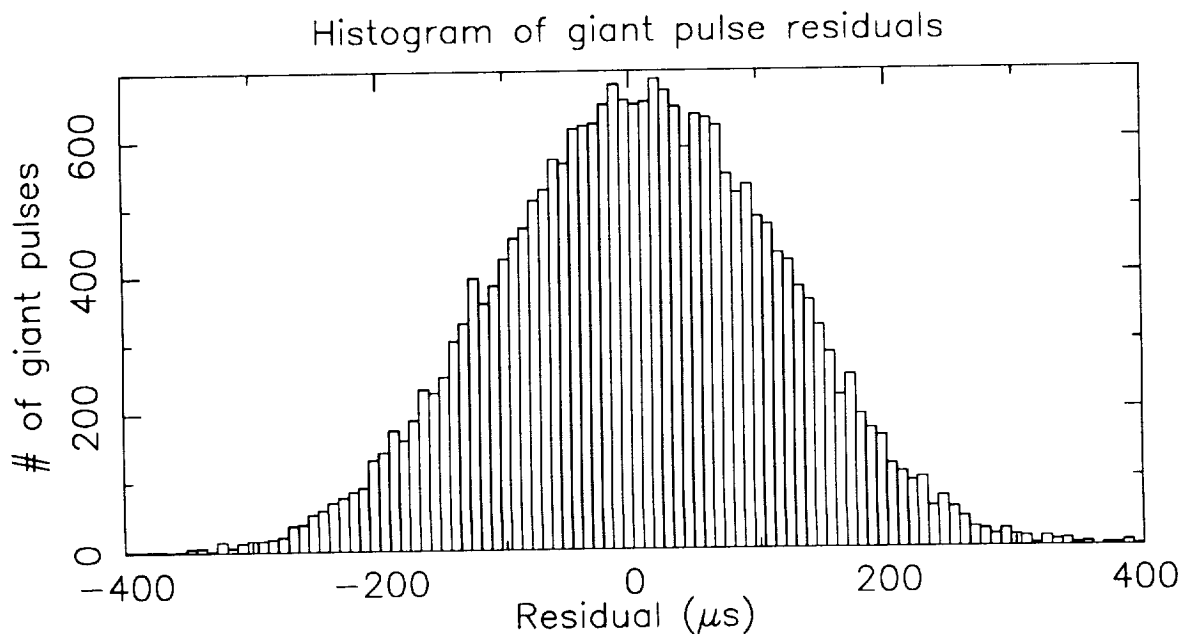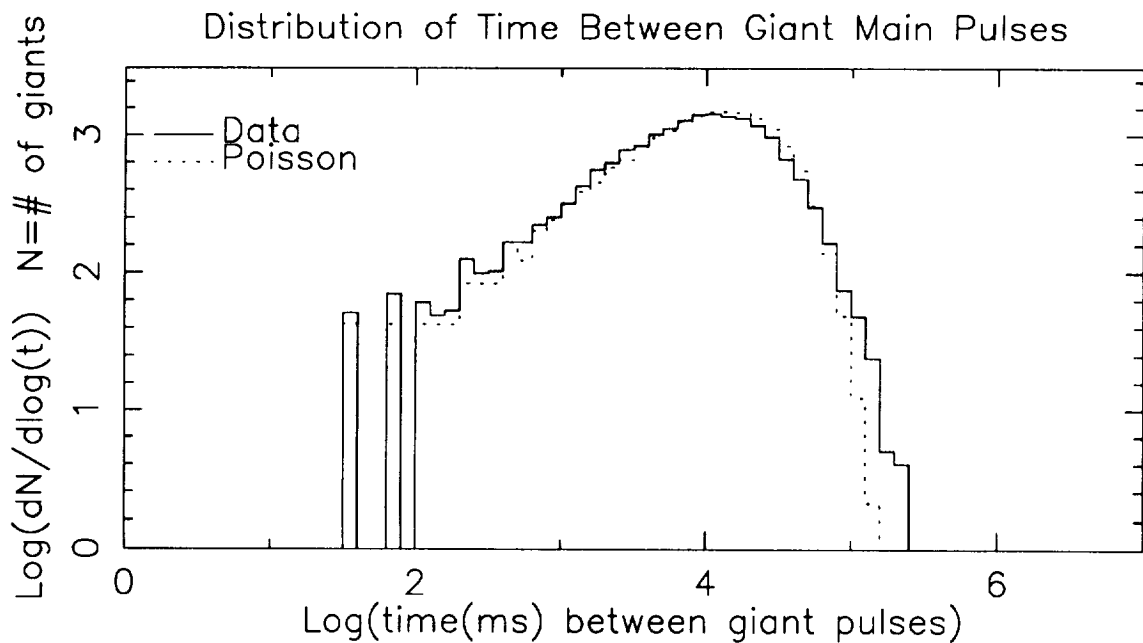
Histogram of giant pulse residuals

Figure 2b shows a histogram of giant pulse arrival time residuals.

Figure 3 We plotted a histogram of the time between giant pulses at 812.5 MHz, using a logarithmic scale with logarithmic bins. The two spikes at 1.5 and 1.8 correspond to one period and two period separation respectively. The dotted curve is a theoretical prediction, $dN/dt = N/t_0 \times \exp(-t/t_0)$, where N=# of giant pulses and t_0 =average time between giant pulses. The exponential distribution has been binned in the same manner as the data.
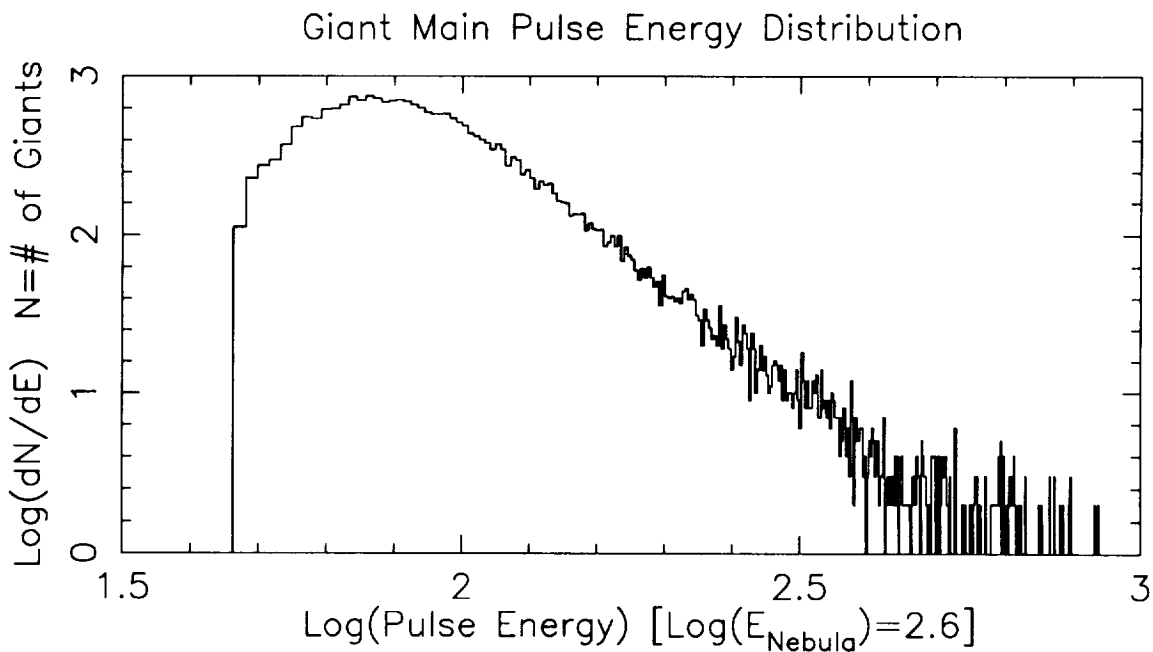

Figure 4: Histogram of giant pulse energies at 812.5 MHz plotted logarithmically.

pulse averages. Detection of correlations, anti-correlations, or uncorrelated results will constrain pulsar emission theories, distinguishing between fluctuations in the pair production cascades and changes in the effectiveness of radio coherence mechanisms.

For a giant pulse arrival time file contact us by email at lundgren@astrosun.tn.cornell.edu or contact Mel Ulmer at ULMER@ossenu.astro.nwu.edu.

References

Argyle, E. 1973, *Ap. J.*, **183**, 973-975.

Argyle, E. and Gower, J.F.R. 1974, *Ap. J.*, **175**, L89-L91.

Backer, D.C. 1970, *Nature*, **228**, 1297.

Bartel, Sieber and Wolszczan, A. 1980, *AA*, **90**, 58-64.

Gower, J.F.R. and Argyle, E. 1972, *Ap. J.*, **171**, L23-L26.

Hankins, T.H. and Rickett, B.J. 1975, *Methods in Computational Physics*, **14**, 55

Hegyi, D., Novick, R., and Thaddeus, P. 1971, *IAU Symp.*, **46**, "The Crab Nebula", p129-140.

Heiles, C., Campbell, D., and Rankin, J. 1970, *Nature*, **226**, 529-531.

Hesse, Wielebinski 1974, *AA*, **31**, 409-413.

Manchester, R.N. and Taylor, J.H. 1977, *Pulsars*, W.H. Freeman and Company, 137-146.

Ritchings, R.T., *MNRAS*, **176**, 249-263.

Staelin, D.H. and Sutton, J.M. 1970, *Nature*, **228**, 69.